Transactions on Electrical and Electronic Materials
https://doi.org/10.1007/s42341-024-00551-2

Online ISSN 2092-7592
Print ISSN 1229-7607

REGULAR PAPER

Modified Dosimetric Features of New Type of Lithium Borate Glass System: Role of Magnesium and Gold Co-doping

Hayder. K. Obayes[1] · **Mohanad H. Meteab**[1] · **Bairaq Abd Al-Kareem**[1]

Received: 19 January 2024 / Revised: 18 May 2024 / Accepted: 22 May 2024

Abstract

The thermoluminescence (TL) behavior of a new type of glass system made up of lithium borate doped with magnesium oxide and gold, known as LB: Mg/Au, was examined. The Mg/Au co-doped LB glasses can contribute to the development of high-performance thermoluminescent dosimetry (TLD) materials for ionizing radiation dose detection and quantification. The composite shows excellent properties compared to other TLD materials. The concentrations of MgO and Au varied from 0.4 to 1 mol% and 0.01–0.07 mol%, respectively. We produced the glasses through the melt-quenching process and then characterized them to evaluate the influence of dopant concentration variation on the TL properties. All samples exhibited a single broad peak ranging between 175 and 196 °C, with the sample made up of 15 mol% Li, 0.03 mol% Au, and 0.8 mol% Mg displaying an optimum TL response. Moreover, the glass that contained 0.03 mol% of Au had the highest TL intensity. The glass showed minimum fading, best linearity, and excellent reproducibility; the XRD profiles of the samples showed their true amorphous nature, while the FESEM morphology displayed their surface homogeneity and excellent transmittance. The DTA curve of the samples revealed that their glass transition, crystallization, and melting peaks were at 500–600, and 700 °C, respectively. The proposed glass composition could prove useful as radiation dosimeters.

Highlights

- Dosmetric features of LB glass is notably modified vie Magnesium /Gold Co-doping.
- For the first time LBMg and LBMgAu synthesis.
- Affecting of annealing and heating rate on glow carve.
- This glass shows excellent sensitivity, great linearity and extremely low fading over dose range.
- Excellent reproducibility, suggesting their potential a radiation dosimeter material.
- These new glass compositions are prospective for ionizing radiation measurements.

✉ Hayder. K. Obayes
hayder.physics1@gmail.com

[1] Directorate General of Education in Babylon Governorate, Ministry of Education, Babylon, Iraq51001

Published online: 16 June 2024

Graphical Abstract

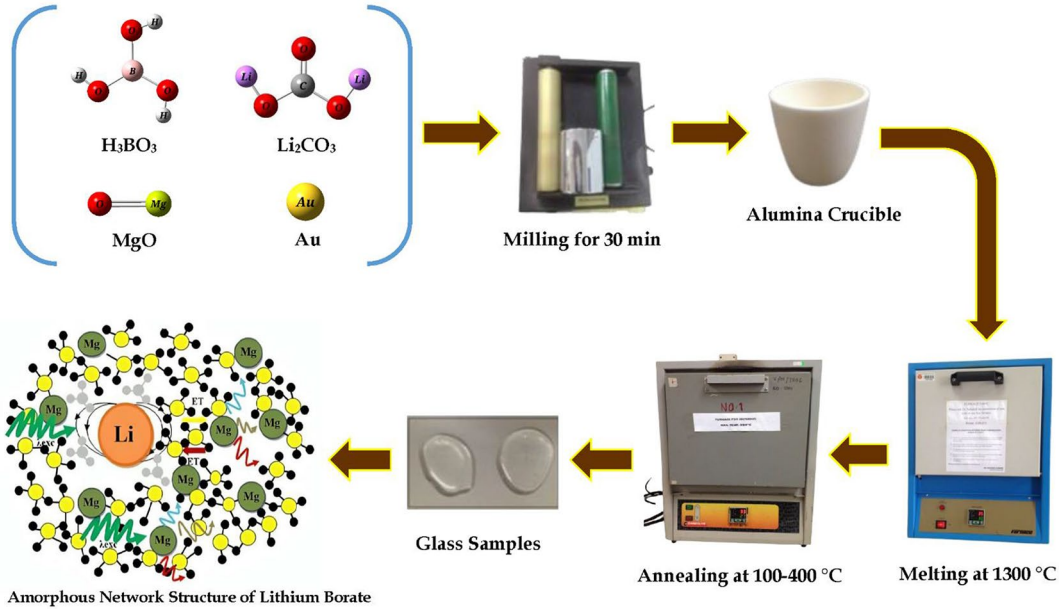

Keywords Co-doping · Dosimetry · LB:Mg/Au · Peak intensity · Thermoluminescence

1 Introduction

Commercially, the TL dosimeters are expensive at the present time, complex in terms of their reuse, suffer from permanent radiation damages [1], and sensitive to the temperature of heat treatment [2]. To overcome these drawbacks many studies have been performed to produce borate glass-based efficient TL materials. Borates show high chemical stability and compatible with diverse TL sensitizers like trivalent rare earth elements, copper, and manganese. In addition, borate glasses display excellent sensitivity, linearity, and storage by overcoming the shortcomings related to fading, light, humidity, and so on. Amongst all borate-based glass system lithium borate (LB) glasses with various dopants reveal superior physical and TL characteristics effective for radiation dosimeter applications [3]. However, there is a need to improve the TL dosimetric performance of such doped and co-doped LB glass system.

Recently, properties of lithium borate [LiB_3O_5] thermoluminescent have also attracted many scientists and researchers attentions for the purposes of medical applications, due to their effective atomic number, which is very close to the biological tissue [4]. The present study focuses to identify some TL properties of lithium borate glass prepared with different compositions of Li_2CO_3 and H_3BO_3 [5]. First studied the TL dosimeter (TLD) traits of LB glass, wherein such glass was made from Li_2CO_3 and H_3BO_3 mixture at 950 °C by melt-quenching approach. Then, the obtained glasses were crystallized via heating at 650 °C and the dopants were incorporated [1, 6]. The TLD features of LB glasses in which the sample made with 15 mol% of Li_2BO_3 and 85 mol% of H_3CO_3 displayed the best TL response, tissue equivalence, excellent sensitivity and linearity under 10 Gy gamma ray irradiation [7]. The optical absorbance of rare earths doped lithium tetra-borate glasses. Melt-quenched glass system with 15 mol% of Li_2CO_3 and 85 mol% of H_3BO_3 were doped using 0.1 mol% of nano-gold to examine their TLD properties. Both undoped and Au-doped glasses were irradiated with Co-60 gamma ray at 1.25 MeV. The results showed a remarkable increase in the TL intensity of these glasses due to Au inclusion [8]. $Li_2B_4O_7$:Sr phosphors were synthesized [9], melt quenching method to determine their TLD properties. Wall et al. also reported the TL response of various lithium borate glasses. Various studied showed that $Li_2B_4O_7$:Cu glasses have excellent TL characteristics and linearity up to 103 Gy thereafter sub-linearity and supra-linearity in response [10–12]. To fulfill the growing demand of high-performance glass-based TLD materials, LB glasses with improved properties are needed.

Researchers have shown that the physicochemical properties of semiconductor materials, such as their size, shape, porosity, and recombination rate suppression efficiency, can control the possibility of removing toxic substances [13]. Currently, metals of transition are becoming developed for the sake of producing glass because of their technological applications potentiality in diverse fields of life including

Table 1 The composition and name of each glass sample

Sample code	Composition (mol%)			
	Li_2CO_3	H_3BO_3	MgO	Au
LBMg	15.0	82.60	0.4	-
LBMg	15.0	82.40	0.6	-
LBMg	15.0	82.20	0.8	-
LBMg	15.0	82.00	1.0	-
LBM0.8Au	15.0	82.19	0.8	0.01
LBM0.8Au	15.0	82.17	0.8	0.03
LBM0.8Au	15.0	82.15	0.8	0.05
LBM0.8Au	15.0	82.13	0.8	0.07

optic, electro, electrochemical, and electronic devices [14–16]. Due to its unique materials structures, borate glass was targeted by various researchers as subjected core in numerous infrared studies.

Some studies indicated that the structural and physical properties of LB glass system can be improved via Au doping wherein white powder of LB can be melted at 917 °C to produce such amorphous structure [17]. LB has density of 2.4 g/cm^3 and solubility is in the range of 1–10%. A simple glow curve and annealing process makes LB glass system attractive for TLD and piezoelectric devices [18]. However, many characteristic parameters (like glow curve, dose linearity and sensitivity) of LB glass system must be refined to apply them as efficient and reliable dosimeters [19]. Based on these factors, we used the standard melt-quenching approach to prepare some LB glasses without Au (coded as LB: Mg) and with Au (coded as LB: Mg/Au) and characterized by various analytical instruments. The role of Mg/Au co-doping one the improved TL properties were determined to explore their possibility for radiation dosimeter fabrication. Results related to the kinetic parameters, fading, linearity, reproducibility, glow curve, and sensitivity were analyzed and presented.

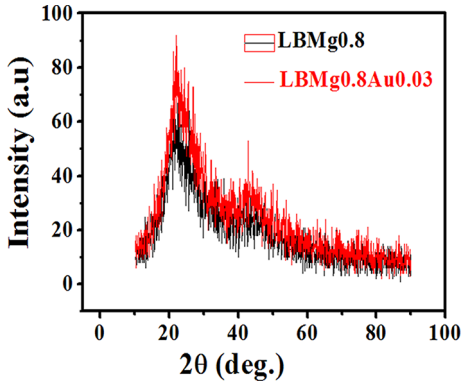

Fig. 1 XRD patterns of selected $LBMg_{0.8}$ and $LBMg_{0.8}Au_{0.03}$ samples

2 Materials and Methods

2.1 Preparation of Glasses

A total of eight glass samples 4 doped with Mg and without Au (LB: Mg) of the form (100-x) $H_3BO_3 + 15Li_2CO_3$ a + xMgO (× = 0.4, 0.6, 0.8 and 1 mol%) and 4 co-doped Au (LB: Mg/Au) of the form (85-y) $H_3BO_3 + 15Li_2CO_3 + 0.8MgO + yAu$ (y = 0.01, 0.03, 0.05, 0 and 0.7 mol% Au) were prepared following the melt-quenching method and characterized at room temperature. LB: Mg glass containing 0.8 mol% of MgO was selected as the optimum sample for further Au doping at different contents. Results revealed that the sample containing 0.03 mol% of Au was optimum. In the process of glass making, pure powders (purchased from Sigma Aldrich) of Li_2CO_3 (99% purity), H_3BO_3 (99.98% purity), MgO (99.9% purity) and Au (98% purity) as raw constituents of the glass were weighed and mixed homogeneously (using milling technique). For each glass batch, the resultant mix was placed in an alumina crucible and melted at $1300°C$ in a furnace (NabGmbHat) for one hour. Once the mixture was completely melted, it was spilt and quenched in a steel mold that was already pre-heated, following that annealing at

Fig. 2 FESEM images of $LBMg_{0.8}$ glass

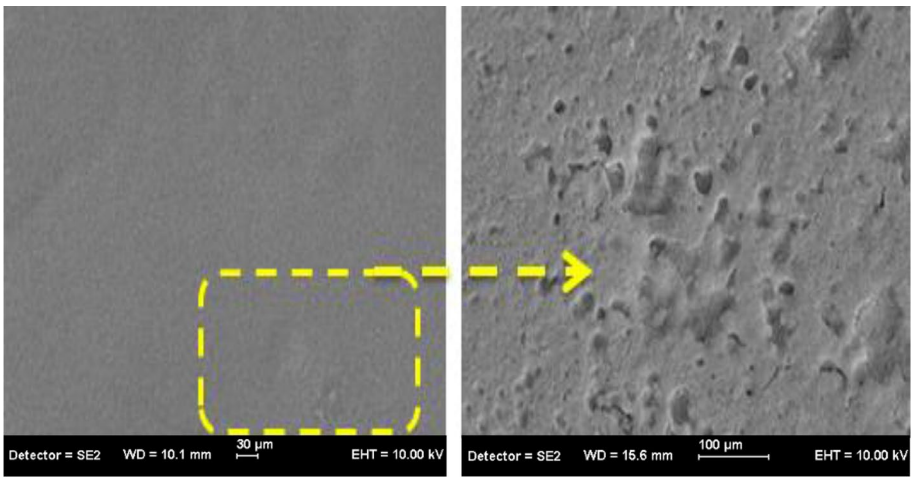

400 °C for 3 h, thus an eliminating of the mechanical stress that can cause glass cracking was resulted. Table 1 details how each prepared sample was composed and named.

2.2 Characterizations of Glasses

The XRD analyses (in the 2θ range of 5°-90° and scanning rate of 0.05 deg./sec) of the samples were conducted using a Siemens Diffractometer (D5000) to confirm their amorphous phase. The diffractometer used Cu Kα line of wavelength $(\lambda) \approx 1.54\ \mathring{A}$, and operated with $40kV$ and $30mA$. FESEM micrographs of the samples were recorded to determine their surface morphology, transmittance, phase purity, and uniformity. The DTA was conducted (Perkin Elmer Pyris Diamond Analyzer worked at 40 kV and 30 mA) to evaluated the temperature of glass transition (T_g), melting (T_m) and crystallization (T_c). The measurement was carried out in the range of 50–1000 °C with a heating rate of 10 °C/min at resolution of ± 0.1 °C. A Har-shaw4500 TLD-reader equipped with A source of gamma rays containing the isotope Co-60 was used to record the samples TL response.

3 Results and Discussions

3.1 XRD Profiles

Figure 1 shows the XRD profiles of the selected two annealed (at 400 °C) samples, wherein the complete absence of any crystalline Bragg peak confirmed their amorphous nature [20, 21]. Besides, the presence of two broad hump around 20–30° and 40–50° corresponded to the weak microcrystalline phases of $LiBO_3$ and $MgBO_3$.

3.2 FESEM Micrographs

Figures 2 and 3 show the FESEM micrographs of the optimum samples $LBMg_{0.8}$ and $LBMg_{0.8}Au_{0.03}$, respectively. The surface morphology of the studied glasses did not display the presence of any granular structures [22, 23], indicating their homogeneous textures. In addition, the glass network structures were appreciably modified due to Au doping.

3.3 DTA Curves

The DTA provided the information of glass thermal properties including T_g, T_m and T_c. The GFA, or glass forming ability, was calculated using the following equation:

$$T_{rg} = \frac{T_g}{T_m} \tag{1}$$

The GFA (T^{rg}) of a glass is considered to be good when $0.5 \leq T_{rg} \leq 0.66$. The obtained excellent values of T_{rg} of the proposed glasses indicated the fulfillment of Kauzmann assumption.

The thermal stability of the glasses were verified by estimating the Hurby parameter [24]:

$$H_g = \frac{T_c - T_g}{T_m - T_c} \tag{2}$$

Glasses with $H_g \leq 0.1$ and $H_g \geq 0.5$ the corresponding thermal stability is considered to be very poor and superior [25]. Table 2 shows the values of glass forming ability and stability of the studied compositions.

Figure 4 depicts DTA results of the studied samples ($LBMg_{0.8}$ and $LBMg_{0.8}Au_{0.3}$) which exhibited T_g at 515 °C and 523 °C (endothermic peaks). The values of T_c (exothermic peaks) were probed at 581 °C and 659 °C. In addition,

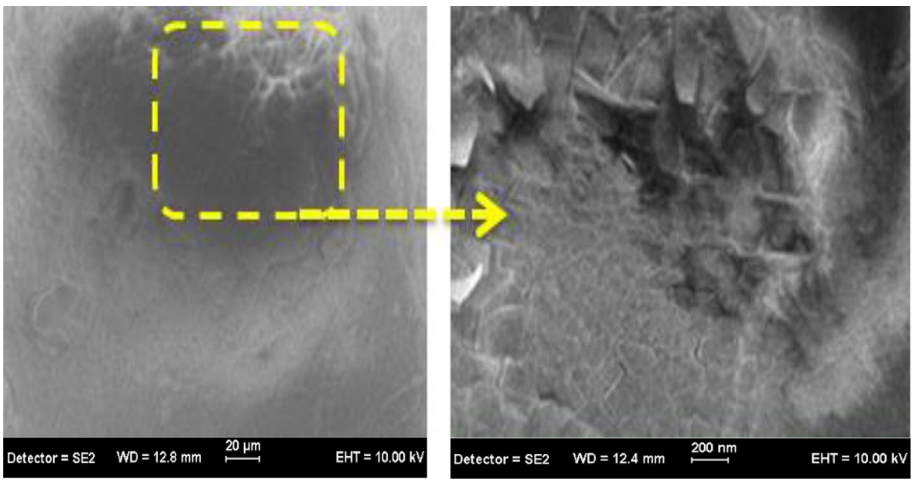

Fig. 3 FE-SEM images of $LBMg_{0.8}Au_{0.03}$ glass

Table 2 Values of GFA and H_g of $LBMg_{0.8}$ and $LBMg_{0.8}Au_{0.03}$ samples

Sample code	T_g (°C)	T_c (°C)	T_m (°C)	T_{rg}	H_g
$LBMg_{0.8}$	515	581	628	0.8	1.4
$LBMg_{0.8}Au_{0.03}$	523	659	761	0.6	1.3

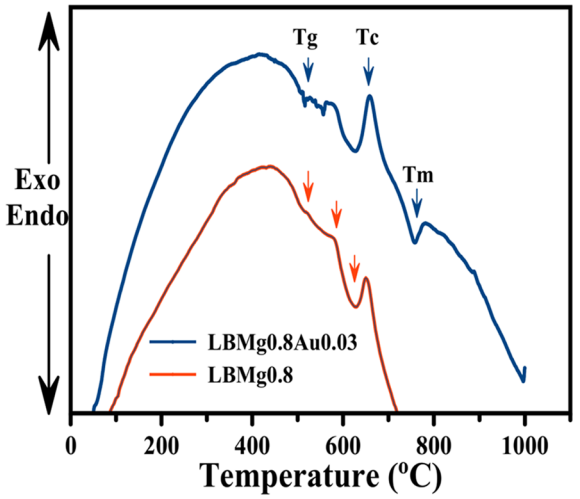

Fig. 4 DTA curves of $LBMg_{0.8}$ and $LBMg_{0.8}Au_{0.03}$

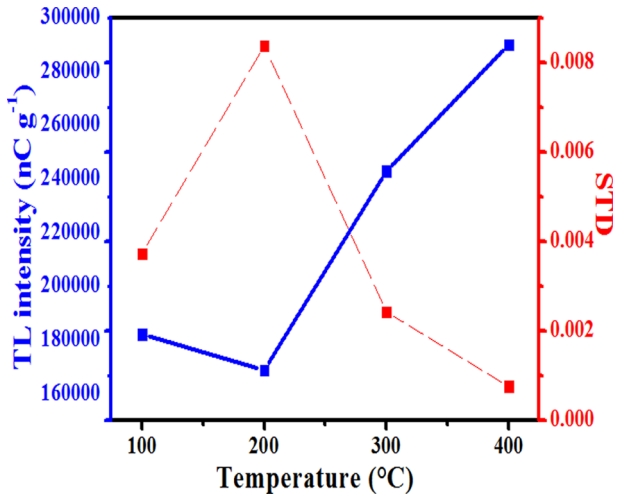

Fig. 5 TL response and STD of $LBMg_{0.8}$ glass against annealing temperature

the values of T_m (endothermic peaks) were observed at 628 °C and 761 °C. The value of T_{rg} and H_g of $LBMg_{0.8}$ and $LBMg_{0.8}Au_{0.3}$ glass was 0.8 and 0.6, respectively.

3.4 Annealing Process

The annealing of the samples was performed to remove all residual TL signal, thus re-establishing the TL sensitivity by eliminating all unstable glow peaks occur at low temperature. Generally, different TL materials show different annealing regime [26, 27]. Before Co-60 gamma radiation exposure of 50 Gy, the proposed glasses were annealed for

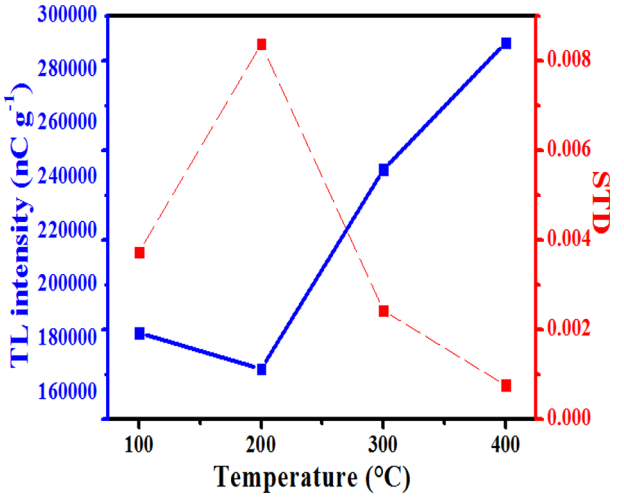

Fig. 6 TL response and STD of $LBMg_{0.8}Au_{0.03}$ glass against annealing temperature

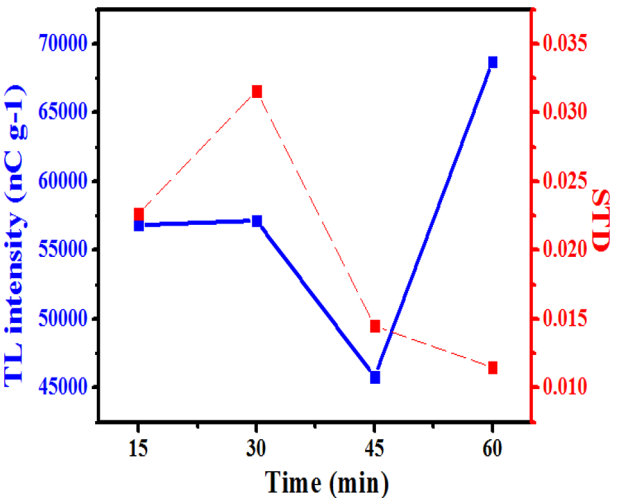

Fig. 7 TL response and STD for $LBMg_{0.8}$ glass against annealing time

(15–60) min ranging in 100–400 °C (an optimization process for pre-irradiation annealing based on temperature and duration). Figures 5 and 6 show how the TL-intensity for $LBMg_{0.8}$ and $LBMg_{0.8}Au_{0.03}$ changes with the annealing temperature, respectively. The glasses annealed at 400 °C displayed the minimum level of standard error and the maximum degree of TL-intensity [28, 29], selecting the value for pre-irradiation annealing of both samples.

Figures 7 and 8 show the dependence of TL intensity and STD for $LBMg_{0.8}$ and $LBMg_{0.8}Au_{0.03}$ glass on annealing temperatures, respectively. Maximum reproducibility (low STD) and TL intensity for $LBMg_{0.8}$ and $LBMg_{0.8}Au_{0.03}$ glasses were correspondingly observed at 60 min and 45 min. For the whole investigation, these pre-irradiation annealing procedures were applied.

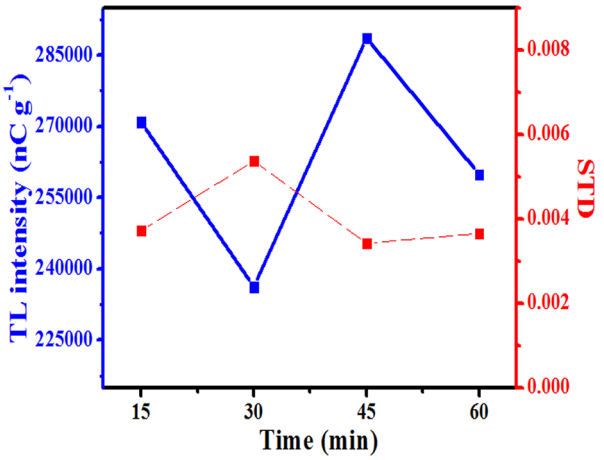

Fig. 8 TL response and STD of $LBMg_{0.8}Au_{0.03}$ glass against annealing time

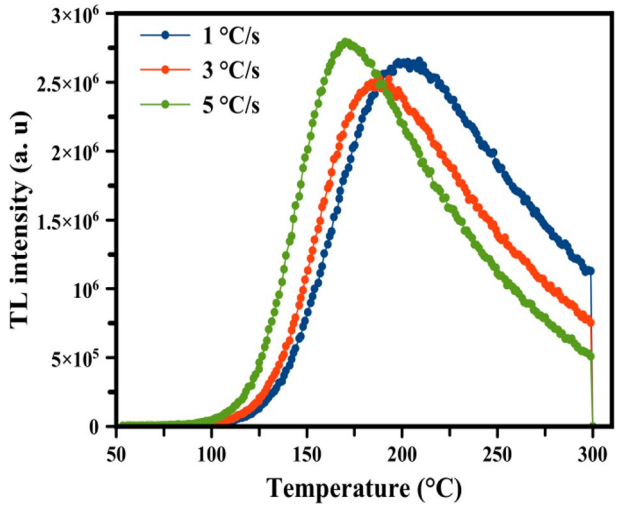

Fig. 9 Heating rate dependence of the TL glow curve for $LBMg_{0.8}$

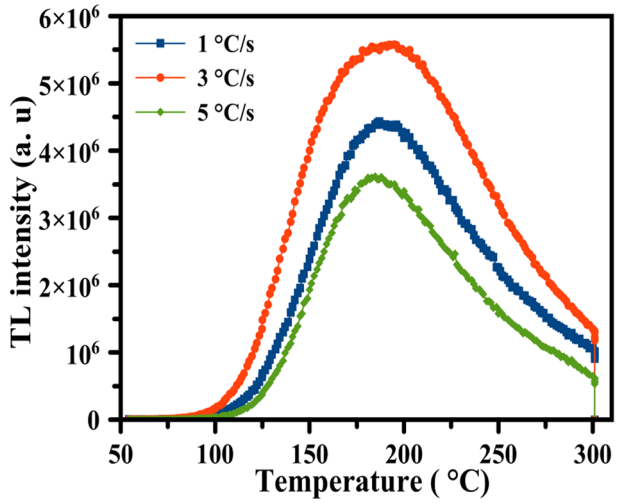

Fig. 10 Heating rate dependence of the TL glow curve for $LBMg_{0.8}Au_{0.03}$

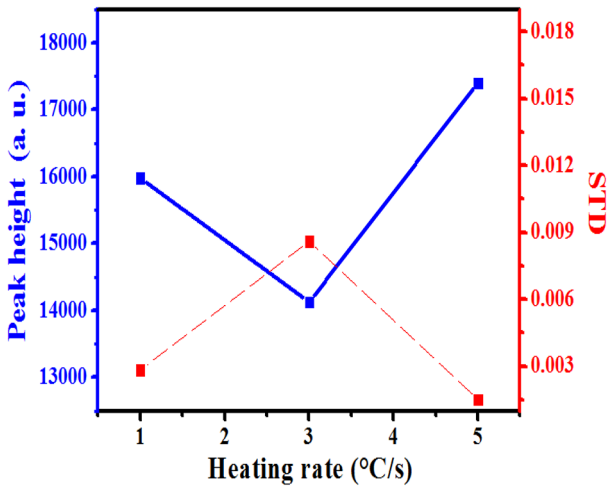

Fig. 11 The dependent TL glow peak intensity and STD of $LBMg_{0.8}$ glass heating rate

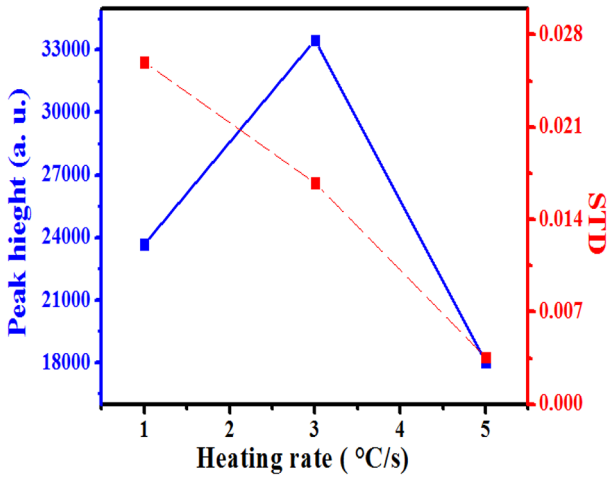

Fig. 12 The dependent TL glow peak intensity and STD of $LBMg_{0.8}Au_{0.03}$ glass heating rate

3.5 Heating Rate Optimization

Figures 9 and 10 show the heating rate dependence of the TL glow curve for $LBMg_{0.8}$ and $LBMg_{0.8}Au_{0.03}$ glasses, respectively under the exposure of 50 Gy Co-60 gamma radiation. The peak intensity was amplified with the raise of heating rate. In short, the approved heating rate of the TLD reader decided the TL intensity of the glow curve.

Figures 11 and 12 show the TL glow peak intensity and STD corresponding to $LBMg_{0.8}$ and $LBMg_{0.8}Au_{0.03}$ measured at various heating rates. Each measurement was performed 5 times and the mean value was estimated to get the STD. Ideally, a best heating rate setting in a minimum standard deviation (STD) of the dosimeter output data and an optimal TL response are required from the TL measurement. In the present glass, the maximum TL response and

minimum STD $LBMg_{0.8}$ and $LBMg_{0.8}Au_{0.03}$ were found at $5°C.s^{-1}$, and $3°C.s^{-1}$, respectively [30].

3.6 TL Glow Curve

Both peak position and shape of the glow curve are important to determine the nature of trap states and fading attributes of a material used for dosimeter fabrication, thus providing an insight regarding the TL mechanism. Figure 13 depicts the TL glow curves of the LBMg glasses under 50 Gy Co-60 gamma ray exposures, which displayed a broad peak at 205 °C. Figure 14 displays the TL peak intensity and STD of the LBMg glasses as a function of Mg ions contents. The $LBMg_{0.8}$ glass exhibited the highest TL peak intensity. This can be attributed to the recombination of excited electrons, which originated from the valence band, with the defects induced by irradiation [31].

Figure 15 shows the TL glow curves of the $LBMg_{0.8}Au$ glasses under 50 Gy Co-60 gamma ray exposures, which revealed an intense peak at 196 °C. Sample $LBMg_{0.8}Au_{0.03}$ showed the maximum TL peak intensity. Figure 16 TL peak intensity and STD as a function of Au contents.

Figure 17 compares the TL glow curve of $LBMg_{0.8}$ glass with that of $LBMg_{0.8}Au_{0.03}$. The TL peak intensity was improved by a factor of 1.3 due to the inclusion Au into the $LBMg_{0.8}$ glass. The $LBMg_{0.8}Au_{0.03}$ glass showed the optimum TL peak intensity. In addition, the observed decrease of the TL peak intensity at Au contents above 0.03 mol% is due to concentration dependent quenching mechanism [32].

3.7 Kinetic Parameters

The observed alteration in the TL glow curves shapes, peak positions, and peak intensities are determined by the trap states in the material [33]. Thus, the kinetic parameters of the dosimeter material like activation energy (E) or trap depth, frequency factor (s), geometric factor (μ_g) and kinetic order (b) strongly depend on the TL mechanisms that decide glow curve characteristics. In this work, the peak shape (also called Chen's method) and initial rise approach was applied to determine the values of E and s for the proposed glasses [34]. The precision of these approaches depend on the characteristics TL glow curve peak temperature (T_m), and the temperatures T_1 and T_2 connected to the FWHM of the TL peak [35].

3.7.1 Peak Shape Method

Figures 18 and 19 display the peak shape method to estimate the kinetic parameters of $LBMg_{0.8}$ and $LBMg_{0.8}Au_{0.03}$ glass, respectively. The following relations were used to compute the geometric factors [35]:

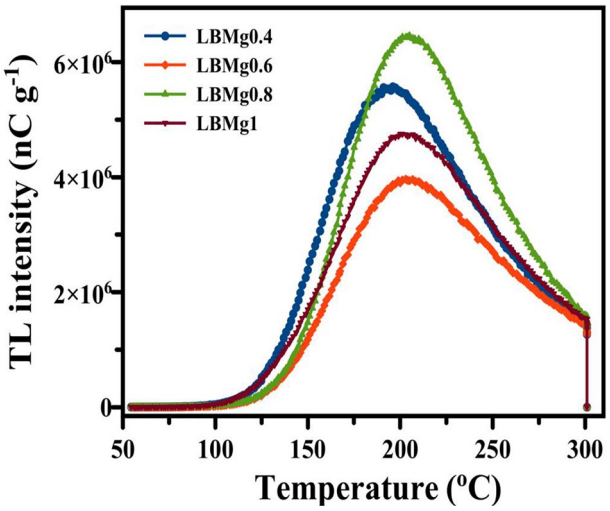

Fig. 13 Glow curves of the LBMg glasses

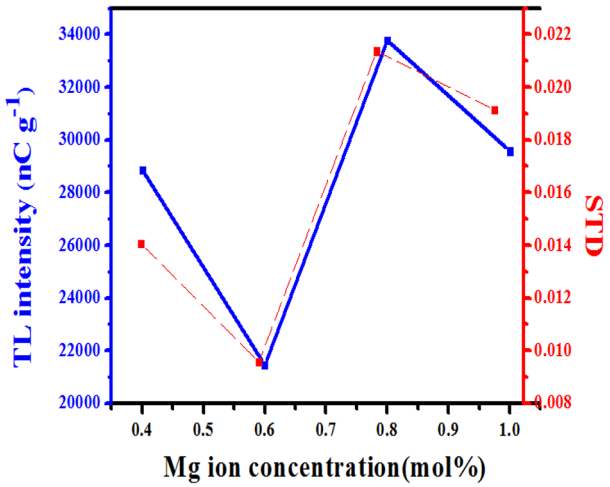

Fig. 14 TL peak intensity and STD of the glasses against Mg ion contents

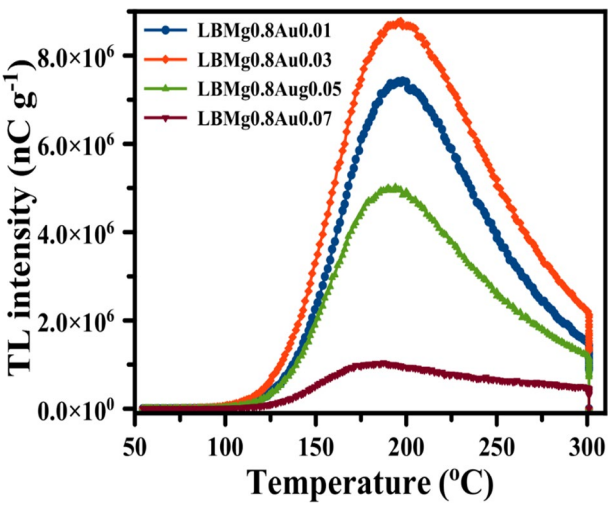

Fig. 15 TL glow curves of $LBMg_{0.8}Au$ glass

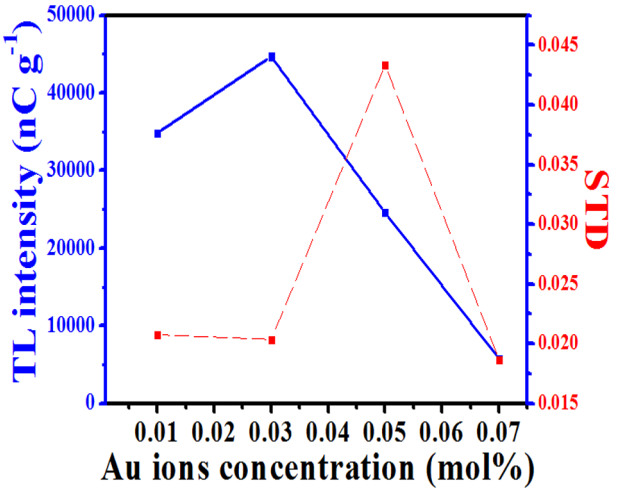

Fig. 16 TL peak intensity and STD of the glasses against Au contents

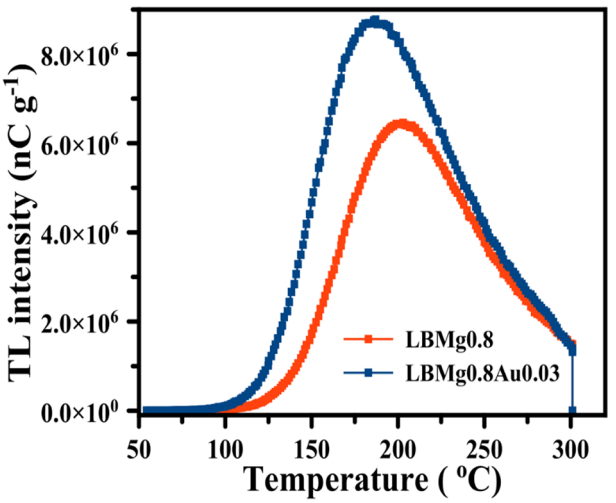

Fig. 17 Glow curves comparison between $LBMg_{0.8}$ and $LBMg_{0.8}Au_{0.03}$ glass

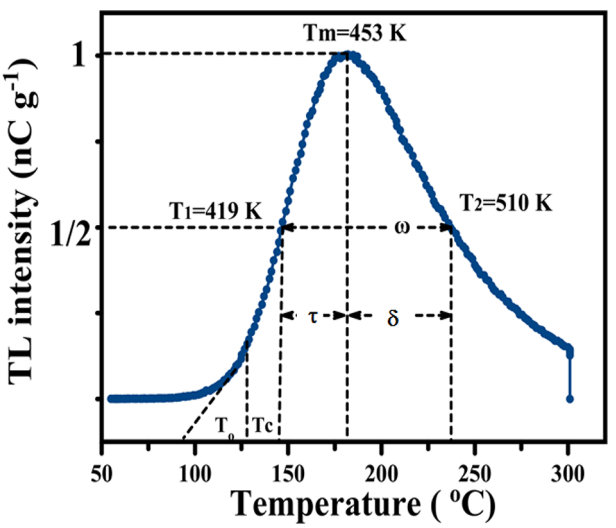

Fig. 18 Peak shape method to estimate the kinetic parameters of $LBMg_{0.8}$ glass

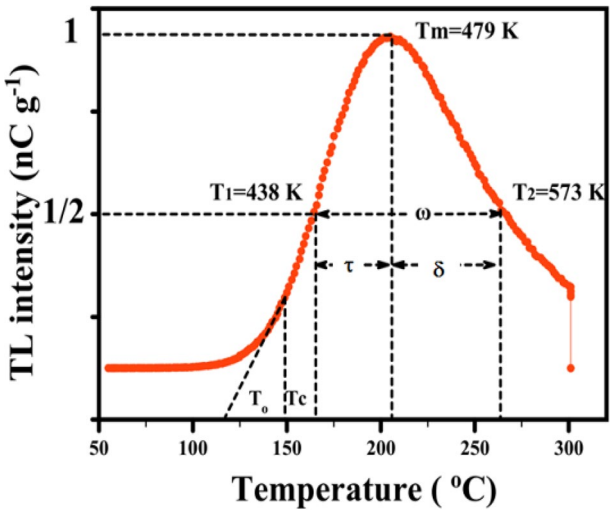

Fig. 19 Peak shape method to estimate the kinetic parameters of $LBMg_{0.8}Au_{0.03}$ glass

$$\mu_g = \frac{T_2 - T_m}{T_2 - T_1} \tag{3}$$

$$\mu_g = \frac{T_2 - T_m}{T_m - T_1} \tag{4}$$

The ideal values of μ_g for the first order and the second kinetics ones are correspondingly ≈ 0.42 and ≈ 0.52. The estimated values of μ_g for $LBMg_{0.8}$ and $LBMg_{0.8}Au_{0.03}$ glasses corresponded to 0.69, and 0.62. Also, Balarin equation [36] was used to evaluate the value to kinetic order:

$$b = 0.0365 \times 10^{2.95\mu_g} \tag{5}$$

The obtained values of b for $LBMg_{0.8}$ and $LBMg_{0.8}Au_{0.03}$ glasses corresponded to 3.96, and 2.46, confirming that the proposed glasses could conform to the second order kinetics. The values of E of the studied glasses were estimated using [37]:

$$E = C_\alpha \frac{k_B T_m^2}{\alpha} - b_\alpha 2 k_B T_m \tag{6}$$

where k_B is the Boltzmann constant, α signifies the τ, δ and ω values as appeared in Figs. 18 and 19. The values of C_α and $b\alpha$ were determined via [37]:

$$C_\tau = 1.510 + 3.0(\mu_g - 0.42), b_\tau = 1.58 + 4.2(\mu_g - 0.42) \tag{7}$$

$$C_\delta = 0.976 + 7.3(\mu_g - 0.42), b_\delta = 0 \tag{8}$$

$$C_\omega = 2.52 + 10.2(\mu_g - 0.42), b_\omega = 1 \tag{9}$$

Table 3 enlists the values of all relevant constants for $LBMg_{0.8}$ and $LBMg_{0.8}Au_{0.03}$ glasses obtained from the Chen's peak shape method. The values of s for the proposed glasses were evaluated using:

$$\frac{\beta E}{kT_m^2} = s\left[1 + (b-1)\frac{2kT_m}{E}\right]\exp\left(-\frac{E}{kT_m}\right) \tag{10}$$

where b and β corresponds to the of kinetics order and rate of linear heating. Table 4 shows the estimated values of frequency factor and thermal activation energy of $LBMg_{0.8}$ and $LBMg_{0.8}Au_{0.03}$ glasses [38].

The observed values of the kinetics parameters of the glasses at various absorbed doses show the continuous energy distribution of the trap states in the material. Herein, E_τ, E_δ and E_ω are the activation energy based on the first half width on the rising side, second half width on the falling side and total width of the glow curve, respectively. It is known that higher energy and higher temperature is needed to de-trap the electrons from deeper traps [39].

3.7.2 Initial Rise Method

The values of E and s of the obtained glasses were computed using Garlick and Gibson initial rise method [40]. This method hypothesized that the change of the trapped carrier population rate is small at the initial part of the TL glow curve ($T << T_m$), The validity of the temperature cut-off is determined by an intensity level that is below 10–15% of the maximum intensity [41]. This method is suitable when the glow curve has clear peak separation. The formula for the intensity of TL radiation (I) is:

$$I(T) = Cexp\left(\frac{-E}{kT}\right) \tag{11}$$

Figures 20 and 21 shows the $ln(ITL)$ linear variation as a function of $(1/kT)$ for $LBMg_{0.8}$ and $LBMg_{0.8}Au_{0.03}$ glasses, respectively.

The values of $_s$ for the glasses were estimated using [42]:

$$S = antilog\left[I - lnA - (b-1)\ln(n_0/N)\right] \tag{12}$$

where A, N, and n_0 is the area under the glow curve, total concentration of traps and initial concentration of the trapped electrons. Assuming the ratio of $n_0/N = 1$ (saturation case) one gets:

$$S = antilog\left(I - lnA - 1\right) \tag{13}$$

Table 5 shows the computed kinetic parameters (E and S) of $LBMg_{0.8}$ and $LBMg_{0.8}Au_{0.03}$ glass obtained using

Table 3 The constant values of c and b for $LBMg_{0.8}$ and $LBMg_{0.8}Au_{0.03}$ glasses

Samples code	Values	τ	δ	ω
$LBMg_{0.8}$	C_α	2.11	2.43	4.56
	b_α	2.42	0.00	1.00
$LBMg_{0.8}Au_{0.03}$	C_α	2.32	2.94	5.27
	b_α	2.71	0.00	1.00

Table 4 Activation energy and frequency factor of $LBMg_{0.8}$ and $LBMg_{0.8}Au_{0.03}$ glass

Samples code	Parameters			
	$E_\tau(eV)$	$E_\delta(eV)$	$E_\omega(eV)$	Average
$LBMg_{0.8}$	0.603	0.618	0.337	0.519
$LBMg_{0.8}Au_{0.03}$	0.717	0.753	0.528	0.666

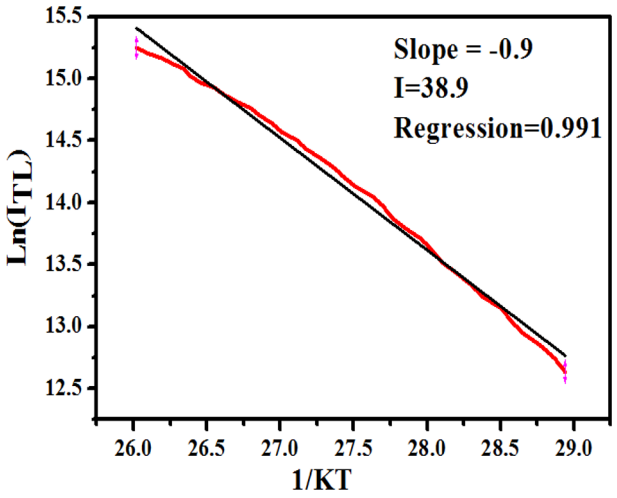

Fig. 20 Evaluation of E for $LBMg_{0.8}$ glass from initial rise plot

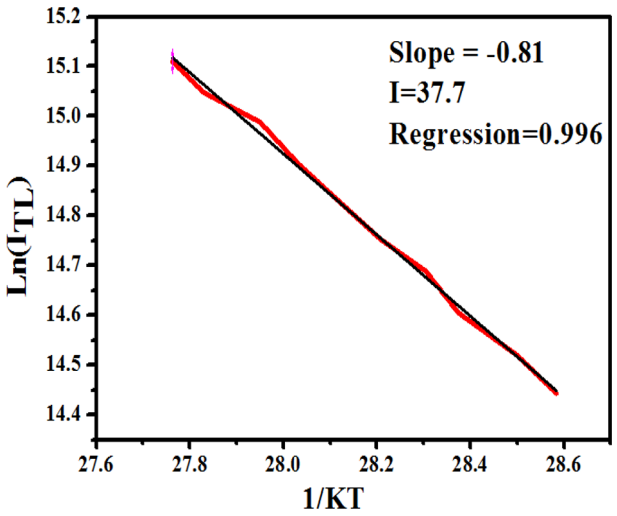

Fig. 21 Evaluation of E for $LBMg_{0.8}Au_{0.03}$ glass from initial rise plot

Table 5 The values E and S for $LBMg_{0.8}$ and $LBMg_{0.8}Au_{0.03}$ glasses

Samples code	Method	E (eV)	s^{-1}
$LBMg_{0.8}$	Peak shape	0.519	0.000059
	Initial rise	0.900	
$LBMg_{0.8}Au_{0.03}$	Peak shape	0.666	0.452000
	Initial rise	0.810	

Table 6 The MDD values of the studied glasses

Sample code	Background STD (nC)	Conversion factor (mGy/nC)	MDD (μGy)
$LBMg_{0.8}$	2.120	1.199×10^{-3}	2.15×10^{-3}
$LBMg_{0.8}Au_{0.03}$	2.255	2.81×10^{-5}	2.32×10^{-5}

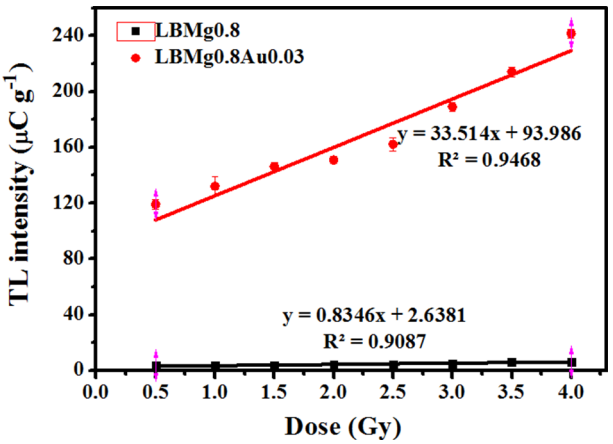

Fig. 22 TL response of $LBMg_{0.8}$ and $LBMg_{0.8}Au_{0.03}$ glasses

two different methods. The slopes of the initial rise plots (Figs. 20 and 21) were used to estimate the values of E and S of the glasses.

3.8 Minimum Detectable Dose

The lowest detection level or minimum detectable dose (MDD) was evaluated using [43]:

$$D_o = (B^* + 2\sigma_B)\,F \tag{14}$$

The variable B^* represents the average background signal of TL resulting from the annealing of samples without irradiation. σ_B represents the average standard error of the background signal, and F represents the calibration factor in units of (Gy TL^{-1}) [44, 45].

The estimated values of MDD, B^*, σ_B, and F for $LBMg_{0.8}$ glass corresponded to $2.15\times10^{3}\mu Gy$, $2.12nC$, $0.0141nC$, and $1.199\times10^{3}mGy.nC^{-1}$. The obtained values of MDD, B^*, σ_B, and F for $LBMg_{0.8}Au_{0.03}$ glass was $2.32\times10^{5}\mu Gy$, $2.255nC$, $0.0.021213nC$, and $2.81\times10^{5}Gy.nC^{1}$, respectively. The value of MDD for $LBMg_{0.8}Au_{0.03}$ glass was lower than $LBMg_{0.8}$ glass, indicating its potential in radiation dosimetry [46]. The values of

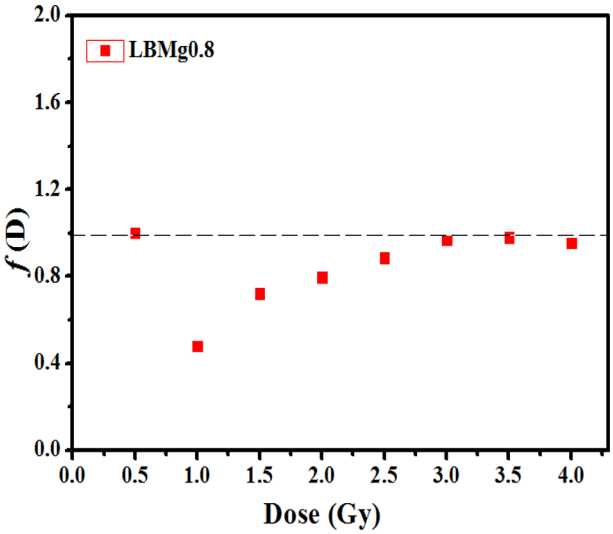

Fig. 23 Plot of $LBMg_{0.8}$ glass (black line is the demarcation line) with dose dependent $f(D)$

the MDD and calibration factor for the optimal glasses that were studied as dosimeter materials are shown in Table 6.

3.9 Dose Response

Figure 22 shows the TL intensity variation of the $LBMg_{0.8}$ and $LBMg_{0.8}Au_{0.03}$ glasses as a function of 0.5 to 4 Gy Co-60 gamma ray exposures, wherein a linear dose response was observed as desired for the accurate dosimetric applications. In addition, the TL response of $LBMg_{0.8}Au_{0.03}$ glass was superior compared to the $LBMg_{0.8}$ glass, indicating an improvement in the TL features of the glasses due to Au codoping.

The normalized dose response (linearity index) of the synthesized glasses was obtained using:

$$f(D) = \frac{TL(D)/(D)}{TL(D_0)/(D_0)} \tag{15}$$

The variable $TL(D)$ reflects the dosage response at a specific dose D, and D_0 represents the lowest dose at which the dose response exhibits a linear form. The linearity index of the suggested glass-based dosimeters is shown in Figs. 23 and 24 [47, 48]. The optimal top-level domain (TLD) material exhibits a $f(D)$ value of 1 across a broad range of doses. The current results confirmed the linear response of the examined TLD composed of $LBMg_{0.8}$ and $LBMg_{0.8}Au_{0.03}$ glasses when subjected to Co-60 gamma radiation within the dose range of 0.5–4 Gy.

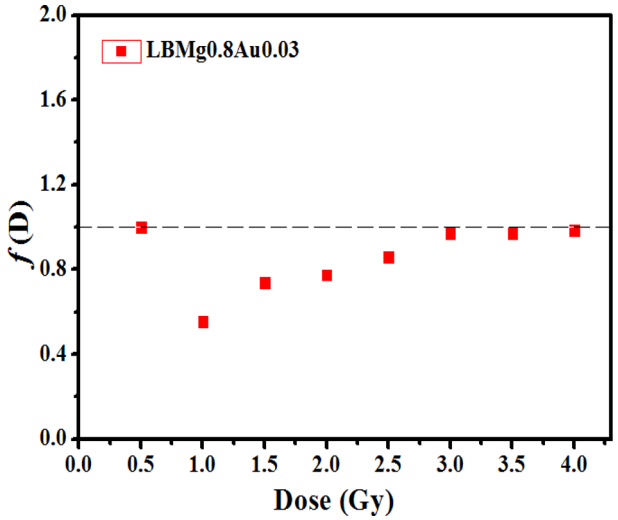

Fig. 24 Plot of $LBMg_{0.8}Au_{0.03}$ glass (black line is the demarcation line) with dose dependent $f(D)$

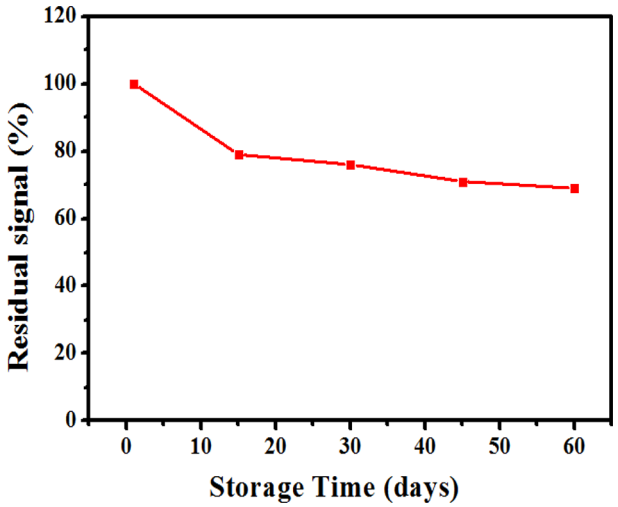

Fig. 25 $LBMg_{0.8}$ glass exposed to 4 Gy thermal fading behavior

3.10 TL Sensitivity

A dosimeter's TL sensitivity is the area of its glow curve divided by the mass and dose ($nCg^{-1}.Gy^{1}$) [49]. The values of the sensitivity for the studied $LBMg_{0.8}$ and $LBMg_{0.8}Au_{0.03}$ glasses (calculated from the slope of Fig. 22) were 0.834 μC $g^{-1}Gy^{-1}$ and 33.51 μC $g^{-1}Gy^{-1}$, respectively. In the studied dose range, the sensitivity of $LBMg_{0.8}Au_{0.03}$ glass was approximately 40 times higher than that of $LBMg_{0.8}$ glass.

3.11 Thermal Fading

Figures 25 and 26 depict the thermal fading characteristics corresponding to $LBMg_{0.8}$ and $LBMg_{0.8}Au_{0.03}$ glass when irradiated with 4 Gy gamma ray dose. The thermal fading of $LBMg_{0.8}$ and $LBMg_{0.8}Au_{0.03}$glasses was determined after

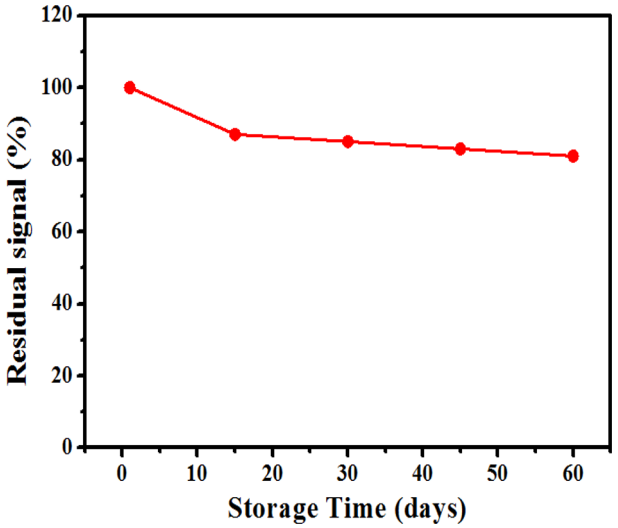

Fig. 26 $LBMg_{0.8}Au_{0.03}$ glass exposed to 4 Gy thermal fading behavior

annealing and irradiation process at a constant dose of 4 Gy followed by storage in the dark conditions at room temperature, reducing the background illumination. After one day of the dose exposure, the readout was started and sustained till 2 months. Identical conditions were maintained to conduct all measurements (several samples), during which the TL response showed a tiny drop while the measurement was underway. Ten days later, the thermal fading for $LBMg_{0.8}$ glass was 15%, one month later it was 21%, and two months later it was 28%. On the other side, $LBMg_{0.8}Au_{0.03}$ glass exhibited 10% thermal fading after 10 days, 16% after one month, and 21% after two months. The observed slight better fading of the co-doped glass may be due to the irradiation-induced creation of defects on phosphor and generation of new trap states [50].

3.12 Reproducibility

Ten specimens of each $LBMg_{0.8}$ and $LBMg_{0.8}Au_{0.03}$ glass were repetitively irradiated with $4Gy$ gamma ray with appropriate preliminary annealing, obtaining their TL signals after every irradiation cycle [51]. Figure 27 show the normalized TL intensity as a function of number of measurements. The results showed a decrease in the reproducibility by approximately 1.25% per cycle for $LBMg_{0.8}$ glass and 1.07% per cycle for $LBMg_{0.8}Au_{0.03}$ glass with STD value below 2%, indicating the reusability $LBMg_{0.8}Au_{0.03}$ glass as dosimetric material [52].

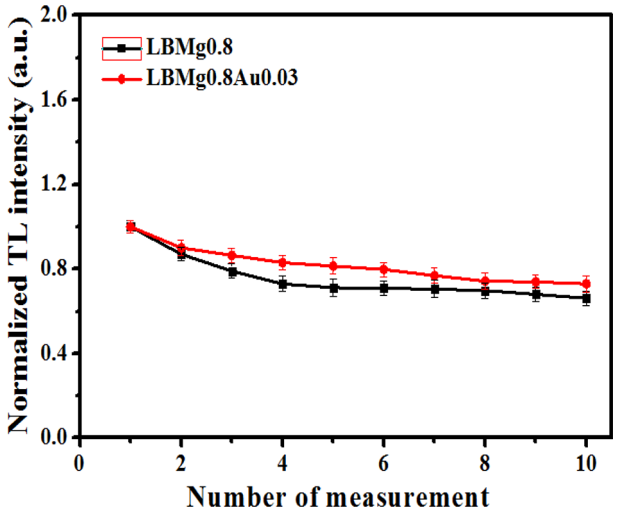

Fig. 27 Reproducibility of $LBMg_{0.8}$ and $LBMg_{0.8}Au_{0.03}$ glass

4 Conclusion

The TL characteristics of two types of LB glasses with MgO doping and MgO/Au co-doping at various contents were studied to determine their potential application in reusable dosimeters. It was shown that the TL features of LB glasses can be improved appreciably by tuning the concentrations of Au/MgO co-doping. All the produced glasses displayed good dose response linearity, reproducibility of the signals, simple glow curve show very slow fading of the signals. suggesting their potential a radiation dosimeter material. The structural and morphological characteristics of the glasses verified their suitability as reusable dosimeter. The DTA results confirmed an excellent thermal stability of the glasses. The inclusion of Au found to induce many new trap states and luminescence centers for recombination by raising the energy levels of the surrounding oxygen ions to the top of the valence band, thus enhancing the TL properties of the glasses. In brief, the Mg/Au co-doped LB glasses can contribute to the development of high performance TLD material for ionizing of detection and quantification of radiation dose.

Acknowledgements The authors express their gratitude to Universiti Teknologi Malaysia and the University of Babylon for their financial assistance and facilities in accordance with Grant Nos. R.J130000.7826.4F490 and 4F736. Appreciation is expressed by the authors for UTFR grant 21H78.

Author Contributions Hayder. K. Obayes, Mohanad H. Meteab, Bairaq Abd Al-Kareem.

Funding No funding.

Data Availability Yes, the data and material are available.

Declarations

Consent for Publication Consent for Publication.

Human and Animal Rights The authors assert that the paper does not involve any human study participants, and therefore, no permission is necessary. The authors further confirm that they have not previously submitted this original paper in any other form or language.

Conflict of Interest No conflict of interest.

Consent to Participate Consent to participate.

References

1. H.K. Obayes, O. Obayes, Q.S. Kadhim, A. Saidu, M. Almaamori, Improved thermoluminescence and kinetic parameters of new strontium/copper co-doped lithium borate glass system. Nucl. Instruments Methods Phys. Res. Sect. B Beam Interact. Mater. Atoms. **455**, 74–82 (2019). https://doi.org/10.1016/j.nimb.2019.06.028
2. G. Kitis, V. Pagonis, On the need for Deconvolution Analysis of Experimental and simulated thermoluminescence glow curves. Mater. (Basel). **16**, 871 (2023). https://doi.org/10.3390/ma16020871
3. V. Chopra, N. El-Faramawy, S.J. Dhoble, Thermoluminescent study of borates for dosimetric applications. In: Phosphor Handbook. 393–415. Elsevier (2023). https://doi.org/10.1016/B978-0-323-90539-8.00013-9
4. G.I. Efenji, I.S. Mustafa, O.O. Ogunleye, T.H. Khazaalah, N.S. Ezra, H.S. Naeem, H.M. Shariff, M. Jamil, M.F.I.A. Malik, Description and dosimetric features of lithium borate glass doped with transition metals for thermoluminesce, a re-evaluation. Phys. Scr. **98**, 52001 (2023). https://doi.org/10.1088/1402-4896/acc23c
5. P. Murugasen, M. Dhavamurthy, P. Anthoniammal, A.A. Suresh, M. Mohapatra, Structural, optical, and thermoluminescence characterizations of 1 mol% Dy3 + ion-activated fluro boro-phosphate glass for photonic devices. Spectrochim Acta Part. Mol. Biomol. Spectrosc. **308**, 123757 (2024). https://doi.org/10.1016/j.saa.2023.123757
6. A. Saidu, H. Wagiran, M.A. Saeed, H.K. Obayes, A. Bala, F. Usman, Thermoluminescence response of rare earth activated zinc lithium borate glass. Radiat. Phys. Chem. **144**, 413–418 (2018). https://doi.org/10.1016/j.radphyschem.2017.10.004
7. B.V. Padlyak, I.I. Kindrat, V.T. Adamiv, Y.O. Kulyk, I.M. Teslyuk, A. Drzewiecki, I. Stefaniuk, Local structure, spectroscopy and luminescence of the Li2B4O7: Cu, Eu glass. Mater. Res. Bull. **167**, 112432 (2023). https://doi.org/10.1016/j.materresbull.2023.112432
8. H.K. Obayes, H. Wagiran, R. Hussin, M.A. Saeed, Structural and optical properties of strontium/copper co-doped lithium borate glass system. Mater. Des. **94**, 121–131 (2016). https://doi.org/10.1016/j.matdes.2016.01.018
9. P.A. Nagpure, N.S. Bajaj, R.P. Sonekar, S.K. Omanwar, Synthesis and luminescence studies of novel rare earth activated lanthanum pentaborate. Indian J. Pure Appl. Phy. **49**, 799–802 (2011)
10. H.K. Obayes, R. Hussin, H. Wagiran, M.A. Saeed, Strontium ion concentration effects on structural and spectral properties of Li4Sr (BO3) 3 glass. J. Non Cryst. Solids. **427**, 83–90 (2015). https://doi.org/10.1016/j.jnoncrysol.2015.07.026
11. B.A. Doull, L.C. Oliveira, D.Y. Wang, E.D. Milliken, E.G. Yukihara, Thermoluminescent properties of lithium borate,

magnesium borate and calcium sulfate developed for temperature sensing. J. Lumin. **146**, 408–417 (2014). https://doi.org/10.1016/j.jlumin.2013.10.022
12. B. Sanyal, M. Goswami, S. Shobha, V. Prakasan, S.P. Chawla, M. Krishnan, S.K. Ghosh, Synthesis and characterization of Dy3 + doped lithium borate glass for thermoluminescence dosimetry. J. Non Cryst. Solids. **475**, 184–189 (2017). https://doi.org/10.1016/j.jnoncrysol.2017.09.016
13. Z.K. Amirhosseini, R. Monsef, S.A. Ehsanizadeh, W.K.Y. Albahadly, H.S. Majdi, A.A. Amir, A.H. Dawood, M. Salavati-Niasari, Tailoring the photocatalytic activity of novel magnetically separable ZnFe12O19-chitosan bionanocomposites: a green preparation, structural characterization and comparative study. Int. J. Hydrogen Energy. **48**, 37286–37301 (2023). https://doi.org/10.1016/j.ijhydene.2023.06.130
14. X. Zeng, G. Li, J. Zhu, M. Sain, R. Jian, NBR/CR-Based high-Damping Rubber composites Containing Multiscale structures for Tailoring Sound Insulation. Macromol. Mater. Eng. **308**, 2200464 (2023). https://doi.org/10.1002/mame.202200464
15. F.S. Olise, S.B. Ola, F.A. Balogun, Characterisation of clay samples from minerals–rich deposits for thermoluminescence applications. J. King Saud Univ. **30**, 158–167 (2018). https://doi.org/10.1016/j.jksus.2017.01.004
16. A.J.J. Bos, Thermoluminescence as a research tool to investigate luminescence mechanisms. Mater. (Basel). **10**, 1357 (2017). https://doi.org/10.3390/ma10121357
17. O.B. Aljewaw, M.K.A. Karim, N. Effendy, H.M. Kamari, M.H.M. Zaid, N.M. Noor, A.A. Salim, N.M. Isa, A.B.A. Kadir, M.T. Chew, A.I. Abokridiga, Physical, optical and thermoluminescence properties of lithium aluminum borate glass co-doped with Dy2O3. Radiat. Phys. Chem. **209**, 111004 (2023). https://doi.org/10.1016/j.radphyschem.2023.111004
18. Z. Jiang, Y. Zhang, L. Zhang, B. Cheng, L. Wang, Effect of calcination temperatures on photocatalytic H2O2-production activity of ZnO nanorods. Chin. J. Catal. **43**, 226–233 (2022). https://doi.org/10.1016/S1872-2067(21)63832-9
19. B.A. Kumar, P.H. Bindu, Advances in borate- and phosphate-based TL materials for in vivo dosimetry. J. Korean Ceram. Soc. **59**, 537–550 (2022). https://doi.org/10.1007/s43207-022-00240-x
20. M.M. Abdelhamied, W.M. Abd-Allah, A.M. Abdelreheem, The effect of nickel additive and ion irradiation on the structural and optical properties of lithium borate glasses. Inorg. Chem. Commun. **163**, 112309 (2024). https://doi.org/10.1016/j.inoche.2024.112309
21. K.S. Shaaban, A.M. Al-Baradi, Z.A. Alrowaili, A.M. Ali, M.S. Al-Buriahi, E.A.A. Wahab, Structural, thermal, and mechanical characteristics of yttrium lithium borate glasses and glass–ceramics. J. Mater. Sci. Mater. Electron. **32**, 28065–28075 (2021). https://doi.org/10.1007/s10854-021-07158-w
22. A. Saidu, H. Wagiran, M.A. Saeed, Y.S.M. Alajerami, Structural properties of zinc lithium borate glass. Opt. Spectrosc. **117**, 396–400 (2014). https://doi.org/10.1134/S0030400X14090239
23. A. Askary, N.S. El, Awwad, H.A. Ibrahium, M.E. Moustapha, A.A. Menazea, Structural, thermal, morphological and antibacterial activities of hybrid bio-nanocomposite Chitosan/Au/Bi2O3 for biomedical applications. J. Polym. Res. **29**, 269 (2022). https://doi.org/10.1007/s10965-022-03116-0
24. R. Sharma, A. Kumar, A. Dawar, S. Ojha, A. Mishra, A. Goyal, R. Laishram, V.G. Sathe, R. Srivastava, O.P. Sinha, Liquid phase exfoliation and characterization of few Layer MoS2 and WS2 nanosheets as Channel Material in Field Effect Transistor. Trans. Electr. Electron. Mater. **24**, 140–148 (2023). https://doi.org/10.1007/s42341-023-00429-9
25. O.I. Sallam, R.M. Ahmed, Gamma-irradiated fluorophosphate glasses doped with various transition metals: a spectroscopic study. Opt. Mater. (Amst). **147**, 114624 (2024). https://doi.org/10.1016/j.optmat.2023.114624
26. A.J.J. Bos, Theory of thermoluminescence. Radiat. Meas. **41**, S45–S56 (2006). https://doi.org/10.1016/j.radmeas.2007.01.003
27. V. Thakur, A. Singh, R. Punia, M. Kaur, L. Singh, Effect of BaTiO3 on the structural and optical properties of lithium borate glasses. Ceram. Int. **41**, 10957–10965 (2015). https://doi.org/10.1016/j.ceramint.2015.05.039
28. J.M. Kalita, M.L. Chithambo, The effect of annealing and beta irradiation on thermoluminescence spectra of α-Al2O3: C, mg. J. Lumin. **196**, 195–200 (2018). https://doi.org/10.1016/j.jlumin.2017.12.036
29. R.R. Dawam, M.L. Chithambo, Thermoluminescence of annealed synthetic quartz: the influence of annealing on kinetic parameters and thermal quenching. Radiat. Meas. **120**, 47–52 (2018). https://doi.org/10.1016/j.radmeas.2018.06.004
30. S. Saha, H.J. Kim, A. Khan, D.J. Daniel, R. Absar, R. Barman, P. Aryal, J. Kaewkhao, S. Kothan, Luminescence and Scintillation properties of Dy3 + doped Li6Y(BO3)3 crystal. Opt. Mater. (Amst). **106**, 109973 (2020). https://doi.org/10.1016/j.optmat.2020.109973
31. J.M. Kalita, M.L. Chithambo, Thermoluminescence of α-Al2O3: C, mg: kinetic analysis of the main glow peak. J. Lumin. **182**, 177–182 (2017). https://doi.org/10.1016/j.jlumin.2016.10.031
32. C.M. Sunta, Kinetics analysis of TL Glow curves. *Unraveling Thermoluminescence*. Springer Series in Materials Science, 202. Springer, New Delhi. (2015). https://doi.org/10.1007/978-81-322-1940-8_4
33. R. Cao, Y. Ye, Q. Peng, G. Zheng, H. Ao, J. Fu, Y. Guo, B. Guo, Synthesis and luminescence characteristics of novel red-emitting Ba2TiGe2O8: Mn4 + phosphor. Dye Pigment. **146**, 14–19 (2017). https://doi.org/10.1016/j.dyepig.2017.06.061
34. A.M. Sadek, G. Kitis, A critical look at the kinetic parameter values used in simulating the thermoluminescence glow-curve. J. Lumin. **183**, 533–541 (2017). https://doi.org/10.1016/j.jlumin.2016.12.002
35. R. Chen, Glow curves with general order kinetics. J. Electrochem. Soc. **116**, 1254 (1969). https://doi.org/10.1149/1.2412291
36. R. Chen, J.L. Lawless, V. Pagonis, Thermoluminescence associated with two-electron traps. Radiat. Meas. **99**, 10–17 (2017). https://doi.org/10.1016/j.radmeas.2017.03.002
37. J.J.M. Órfão, Review and evaluation of the approximations to the temperature integral. AIChE J. **53**, 2905–2915 (2007). https://doi.org/10.1002/aic.11296
38. C. Manjunath, M.S. Rudresha, K.R. Nagabhushana, R.H. Krishna, B.M. Nagabhushana, B.M. Walsh, Thermoluminescence glow curve analysis of gamma irradiated Sr2SiO4:Dy3 + nanophosphor. Phys. B Condens. Matter. **585**, 412113 (2020). https://doi.org/10.1016/j.physb.2020.412113
39. A.M. Sadek, H.M. Eissa, A.M. Basha, G. Kitis, Resolving the limitation of the peak fitting and peak shape methods in the determination of the activation energy of thermoluminescence glow peaks. J. Lumin. **146**, 418–423 (2014). https://doi.org/10.1016/j.jlumin.2013.10.031
40. A.M. Sadek, H.M. Eissa, A.M. Basha, G. Kitis, Development of the peak fitting and peak shape methods to analyze the thermoluminescence glow-curves generated with exponential heating function. Nucl. Instruments Methods Phys. Res. Sect. B Beam Interact. Mater. Atoms. **330**, 103–107 (2014). https://doi.org/10.1016/j.nimb.2014.04.006
41. N.S. Rawat, M.S. Kulkarni, D.R. Mishra, B.C. Bhatt, C.M. Sunta, S.K. Gupta, D.N. Sharma, Use of initial rise method to analyze a general-order kinetic thermoluminescence glow curve. Nucl. Instruments Methods Phys. Res. Sect. B Beam Interact. Mater. Atoms. **267**, 3475–3479 (2009). https://doi.org/10.1016/j.nimb.2009.08.002

42. C. Furetta, M. Prokic, R. Salamon, V. Prokic, G. Kitis, Dosimetric characteristics of tissue equivalent thermoluminescent solid TL detectors based on lithium borate. Nucl. Instruments Methods Phys. Res. Sect. Accel Spectrometers Detect. Assoc. Equip. **456**, 411–417 (2001). https://doi.org/10.1016/S0168-9002(00)00585-4
43. G. Kitis, A. Sadek, G. Polymeris, V. Pagonis, Simulation of the effect of resolution between thermoluminescence peaks on the initial rise method of analysis. Nucl. Instruments Methods Phys. Res. Sect. B Beam Interact. Mater. Atoms. **524**, 1–7 (2022). https://doi.org/10.1016/j.nimb.2022.05.004
44. M.M. Mair, M. Kattwinkel, O. Jakoby, F. Hartig, The minimum detectable difference (MDD) concept for establishing trust in nonsignificant results: a critical review. Environ. Toxicol. Chem. **39**, 2109–2123 (2020). https://doi.org/10.1002/etc.4847
45. H.K. Obayes, H. Wagiran, R. Hussin, M.A. Saeed, A new strontium/copper co-doped lithium borate glass composition with improved dosimetric features. J. Lumin. **176**, 202–211 (2016). https://doi.org/10.1016/j.jlumin.2016.03.024
46. J.A. Harvey, K.J. Kearfott, M. Rafique, Dose response linearity and practical factors influencing minimum detectable dose for various thermoluminescent detector types. J. Radioanal Nucl. Chem. **303**, 1711–1718 (2015). https://doi.org/10.1007/s10967-014-3794-6
47. R. Kaur, R.B. Rakesh, S.G. Mhatre, V. Bhatia, D. Kumar, H. Singh, S.P. Singh, A. Kumar, Physical, optical, structural and thermoluminescence behaviour of borosilicate glasses doped with trivalent neodymium ions. Opt. Mater. (Amst). **117**, 111109 (2021). https://doi.org/10.1016/j.optmat.2021.111109
48. A. Soni, D.R. Mishra, B.C. Bhatt, S.K. Gupta, N.S. Rawat, M.S. Kulkarni, D.N. Sharma, Thermally assisted OSL: a potent tool for improvement in minimum detectable dose and extension of dose range of Al 2 O 3: C. Geochronometria. **40**, 258–265 (2013). https://doi.org/10.2478/s13386-013-0133-6
49. V. Correcher, J. Garcia-Guinea, T. Rivera, Thermoluminescence sensitivity of daily-use materials. Radiat. Eff. Defects Solids. **164**, 232–239 (2009). https://doi.org/10.1080/10420150902734064
50. J.A. Harvey, N.P. Haverland, K.J. Kearfott, Characterization of the glow-peak fading properties of six common thermoluminescent materials. Appl. Radiat. Isot. **68**, 1988–2000 (2010). https://doi.org/10.1016/j.apradiso.2010.04.028
51. A.O. Elsheikh, A. El-Hafez, M.M. Ahmed, Y.A.-A. Abdul-Razek, M.E. El-Nagdy, Quantification of various factors influencing repeatability and reproducibility of TLD-600 detector. Arab. J. Nucl. Sci. Appl. **53**, 58–66 (2020). https://doi.org/10.21608/AJNSA.2019.13313.1219
52. A. Amarlou, K. Mohammadi, N. Banaee, H.A. Nedaei, Synthesis and evaluation of thermoluminescence properties of ZrO2:mg for radiotherapy dosimetry. Radiat. Environ. Biophys. **60**, 647–652 (2021). https://doi.org/10.1007/s00411-021-00928-4